# Design Constraints for Image-Reject Frequency-Translating $\Delta\Sigma$ Modulators

Philip M. Chopp and Anas A. Hamoui

***Abstract*—This brief derives design constraints for bandpass $\Delta\Sigma$ modulators that use mixers to perform frequency downconversion inside their $\Delta\Sigma$ loop. Such systems, which are referred to as frequency-translating $\Delta\Sigma$ modulators, facilitate direct analog-to-digital conversion (ADC) of high-frequency signals that cannot adequately be processed using classical bandpass $\Delta\Sigma$ modulator architectures. The derived constraints are required for the correct design of frequency-translating $\Delta\Sigma$ modulators: 1) The *sampling* constraints maintain the stability of the $\Delta\Sigma$ feedback loop and prevent the mixing of the undesired signal content into the input-signal band, thereby ensuring that the time-varying behavior of the mixers does not affect the ADC resolution; and 2) the *noise-shaping* constraints minimize performance loss during the recombination of the in-phase and quadrature feedback paths. This brief analyzes frequency-translating $\Delta\Sigma$ modulators that are designed with image-reject (quadrature) mixing and that are implemented using continuous- or discrete-time lowpass or complex-bandpass inner-loop $\Delta\Sigma$ modulators. Thus, the derived constraints offer a valuable reference for the design of image-reject frequency-translating $\Delta\Sigma$ ADCs.**

***Index Terms*—Analog-to-digital (A/D) conversion, bandpass, frequency translation, sigma–delta ($\Delta\Sigma$) modulation.**

## I. Introduction

BANDPASS $\Delta\Sigma$ modulation is an attractive approach for direct analog-to-digital (A/D) conversion of IF signals. However, due to the technological limitations of CMOS processes and the requirement for a moderate power budget, the maximum input frequency that can be adequately processed using a classical bandpass $\Delta\Sigma$ modulator architecture is limited to approximately 50–60 MHz [1], [2]. To extend the advantages of $\Delta\Sigma$ modulation to high-frequency signals, [3] and [5] proposed the use of frequency downconversion inside the $\Delta\Sigma$ loop. These *downconversion bandpass* $\Delta\Sigma$ modulators perform noise shaping largely at baseband or at a low IF, thereby relaxing the design requirements on the $\Delta\Sigma$ loop filter.

Downconversion bandpass $\Delta\Sigma$ modulators can be split into two categories: 1) *frequency-translating* $\Delta\Sigma$ modulators, which use mixing in their forward path [3], [4]; and 2) *subsampling* $\Delta\Sigma$ modulators, which use undersampling in their forward path [5]–[9]. Both architectures require upconversion mixers in their feedback path.

Manuscript received June 10, 2009; revised September 1, 2009. Current version published December 16, 2009. This work was supported in part by the Natural Sciences and Engineering Research Council of Canada and the Fonds Québécois de la Recherche sur la Nature et les Technologies. This paper was recommended by Associate Editor H.-S. Chen.

The authors are with the Department of Electrical and Computer Engineering, McGill University, Montreal, QC H3A 2A7, Canada (e-mail: anas.hamoui@mcgill.ca).

Digital Object Identifier 10.1109/TCSII.2009.2035266

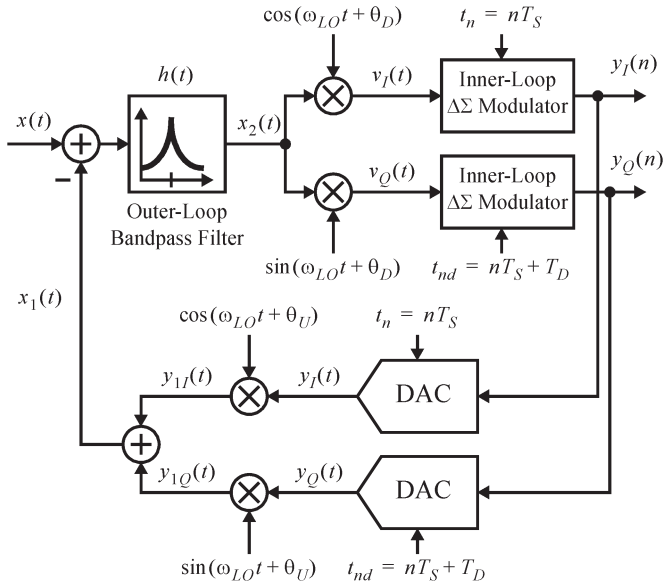


Fig. 1. Frequency-translating $\Delta\Sigma$ modulator with image-reject (quadrature) mixing. Here, $T_S$ is the sampling period, and $T_D$ is the quadrature-path sampling delay.

Frequency-translating $\Delta\Sigma$ modulators have two principal advantages over subsampling $\Delta\Sigma$ modulators: 1) They can use continuous-time (CT) loop-filter stages in their forward path following downconversion mixing, thus suppressing aliasing and sampling errors while offering greater potential for high-speed low-power design; and 2) they do not require wideband sampling switches, thus reducing both design complexity and sampled out-of-band noise.

Fig. 1 depicts a block diagram of the image-reject (quadrature) frequency-translating $\Delta\Sigma$ modulator. Observe that, since the downconversion mixers are inside the $\Delta\Sigma$ loop, mixing nonidealities and any in-phase and quadrature path mismatch are shaped by the outer-loop bandpass filter. This filter is implemented using a single-stage $LC$ resonator, which is suitable for high-frequency signal processing.

When the frequency response of the outer-loop bandpass filter is translated to baseband or to a low IF, its selectivity, and hence its ability to shape quantization noise, is reduced. Therefore, additional $\Delta\Sigma$ loop-filter stages must be included after the downconversion mixers to enhance the overall quantization noise-shaping performance. These inner-loop $\Delta\Sigma$ modulators (Fig. 1) can be realized with lowpass or complex-bandpass loop filters to process zero- or low-IF signals. They are implemented using active-$RC$ or switched-capacitor circuit topologies [10], which facilitate the use of switching mixers.

For the image-reject frequency-translating $\Delta\Sigma$ ADC, this brief derives the following: 1) *sampling* constraints, which maintain the stability of the $\Delta\Sigma$ feedback loop and prevent the mixing of the undesired signal content into the input-signal band; and 2) *noise-shaping* constraints, which minimize performance loss during the recombination of the in-phase and quadrature feedback paths.

The brief is structured as follows. Sections II and III derive the sampling and noise-shaping constraints, respectively. Section IV then validates the derived constraints using system-level behavioral simulations in Simulink.

## II. Sampling Constraints

Mixers are time-varying blocks by definition. When they are inserted into the feedback loop of a $\Delta\Sigma$ modulator (Fig. 1), its loop response also becomes time varying. Therefore, to preserve the stability of the $\Delta\Sigma$ feedback loop and prevent undesired signal content from mixing into the input-signal band, certain constraints must be imposed on the timing of the sampling instants in a frequency-translating $\Delta\Sigma$ modulator. These constraints ensure that, when sampled, the loop response of the frequency-translating $\Delta\Sigma$ modulator is effectively linear time invariant (LTI). A time-varying system whose sampled response is LTI is referred to as a periodically linear time-invariant (PLTI) system [3]. Accordingly, a frequency-translating $\Delta\Sigma$ modulator must be a PLTI system.

Consider the frequency-translating $\Delta\Sigma$ modulator in Fig. 1. Define the in-phase and quadrature sampling instants as

$$t_n = nT_S \quad \text{and} \quad t_{nd} = nT_S + T_D \tag{1}$$

where $T_S$ is the sampling period, and $T_D$ is the quadrature-path sampling delay. This section derives the general relationships between $T_S$, $T_D$, and the period of the local-oscillation (LO) signal $T_{\mathrm{LO}}$ (in Fig. 1) that must be satisfied for correct operation of an image-reject frequency-translating $\Delta\Sigma$ modulator.

### A. Loop Response

The sampling constraints are developed by first deriving the loop response, from $y(t)$ to $v(t)$, of the image-reject frequency-translating $\Delta\Sigma$ modulator in Fig. 1. The sampling period $T_S$ and the quadrature-path sampling delay $T_D$ are then selected, such that the time-varying terms in this loop response are suppressed.

Following upconversion mixing, the summed output of the in-phase and quadrature feedback paths (Fig. 1) is given by

$$x_1(t) = y_I(t)\cos(\omega_{\mathrm{LO}}t) + y_Q(t)\sin(\omega_{\mathrm{LO}}t) \tag{2}$$

where $y_I(t)$ and $y_Q(t)$ represent the outputs of the in-phase and quadrature feedback digital-to-analog converters (DACs), respectively. To keep the derived results tractable, phase terms $\theta_U$ and $\theta_D$ in Fig. 1 are assumed to be 0. Furthermore, subsequent equations only consider the in-phase component $y_I(t)$ (i.e., $y_Q(t)$ is set to 0).

The loop response, from $y(t)$ to $v(t)$, is derived by setting the input signal $x(t)$ to 0. The output of the outer-loop filter $h(t)$ in Fig. 1 is then given by

$$\begin{aligned} x_2(t) &= h(t) \otimes x_1(t) \\ &= \int_{-\infty}^{\infty} h(\tau) y_I(t-\tau)\cos\left(\omega_{\mathrm{LO}}(t-\tau)\right) d\tau \end{aligned} \tag{3}$$

where $\otimes$ represents the convolution operation. By expanding the $\cos(\omega_{\mathrm{LO}}(t-\tau))$ term using standard trigonometric identities, $x_2(t)$ can be rewritten as

$$x_2(t) = x_{2I}(t)\cos(\omega_{\mathrm{LO}}t) + x_{2Q}(t)\sin(\omega_{\mathrm{LO}}t) \tag{4}$$

where

$$x_{2I}(t) = [h(t)\cos(\omega_{\mathrm{LO}}t)] \otimes y_I(t) \tag{5}$$

$$x_{2Q}(t) = [h(t)\sin(\omega_{\mathrm{LO}}t)] \otimes y_I(t). \tag{6}$$

The outputs of the downconversion mixers are then given by

$$v_I(t) = \frac{1}{2}x_{2I}(t)\left[1+\cos(2\omega_{\mathrm{LO}}t)\right] + \frac{1}{2}x_{2Q}(t)\sin(2\omega_{\mathrm{LO}}t) \tag{7}$$

$$v_Q(t) = \frac{1}{2}x_{2I}(t)\sin(2\omega_{\mathrm{LO}}t) + \frac{1}{2}x_{2Q}(t)\left[1-\cos(2\omega_{\mathrm{LO}}t)\right]. \tag{8}$$

Equations (7) and (8), together with (5) and (6), give the effective response, from $y(t)$ to $v(t)$, of the feedback system in Fig. 1. They demonstrate that the loop response of a frequency-translating $\Delta\Sigma$ modulator is not LTI, due to the presence of the $\cos(2\omega_{\mathrm{LO}}t)$ and $\sin(2\omega_{\mathrm{LO}}t)$ terms. To ensure that this loop response is PLTI when sampled, the sampling period $T_S$ and the quadrature-path sampling delay $T_D$ must be selected (as derived next) such that the time-varying terms remain constant across all sampling instants.

### B. Sampling and Delay Constraints

If the in-phase component $v_I(t)$ in (7) is sampled at time instants $t_n = nT_S$ (Fig. 1), with $T_S$ set to an integer multiple of $T_{\mathrm{LO}}/2$, it reduces to $v_I(t_n) = x_{2I}(t_n)$, and hence, time invariance is satisfied. This constraint on the sampling period can be generalized as

$$T_S = k_S\frac{T_{\mathrm{LO}}}{2}, \quad k_S = 1, 2, 3, \ldots. \tag{9}$$

If the quadrature component $v_Q(t)$ in (8) is sampled at time instants $t_n = nT_S$, with $T_S$ selected according to the constraint given in (9), it reduces to $v_Q(t_n) = 0$ in all cases. However, since the quadrature LO signal is $\pi/2$ out-of-phase with respect to the in-phase LO signal, delaying the quadrature-path sampling instants by $T_D = T_{\mathrm{LO}}/4$ and sampling $v_Q(t)$ at time instants $t_{nd} = nT_S + T_D$ (as shown in Fig. 1) results in $v_Q(t_{nd}) = x_{2Q}(t_{nd})$. Accordingly, using (9), the constraint on the quadrature-path sampling delay can be generalized as

$$T_D = \frac{1}{k_S}\frac{T_S}{2}, \quad k_S = 1, 2, 3, \ldots. \tag{10}$$

Observe that, when applying the constraints in (9) and (10), the ratio $T_D/T_S$ decreases as $T_S/T_{\mathrm{LO}}$ increases (i.e., as $k_S$

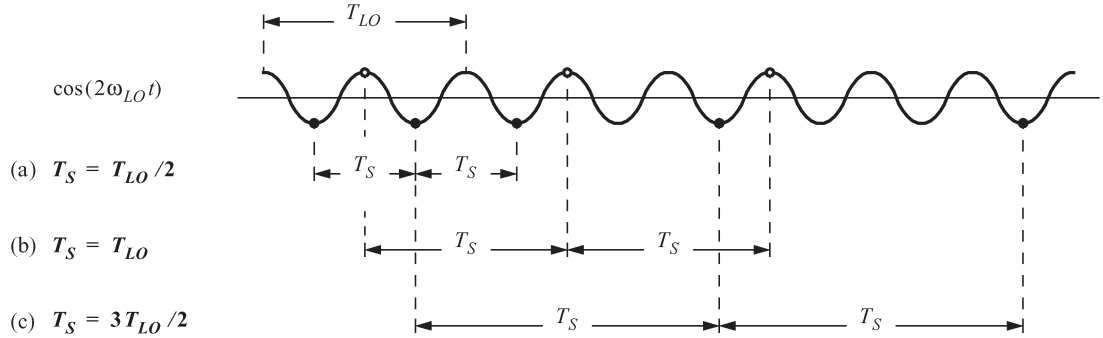


Fig. 2. Timing of the quadrature-path sampling instants $t_{nd}$ for $T_D = T_S/2$ and: (a) $T_S = T_{\rm LO}/2$; (b) $T_S = T_{\rm LO}$; and (c) $T_S = 3T_{\rm LO}/2$.

increases), thereby making it increasingly difficult to accurately implement $T_D$. To solve this problem, the constraint in (9) is revised in the following discussion, such that $T_D$ scales with $T_{\rm LO}$. This makes it possible to adjust $T_S/T_{\rm LO}$ without affecting $T_D/T_S$.

Let the quadrature-path sampling delay be fixed at $T_D = T_S/2$. Consider the case where the sampling period is $T_S = T_{\rm LO}/2$ [i.e., for $k_S = 1$ in (9)]. At the quadrature-path sampling instants $t_{nd} = nT_S + T_D$, $\cos(2\omega_{\rm LO}t_{nd}) = -1$ and $\sin(2\omega_{\rm LO}t_{nd}) = 0$, resulting in $v_Q(t_{nd}) = x_{2Q}(t_{nd})$ in (8). Fig. 2(a) plots the $\cos(2\omega_{\rm LO}t)$ curve, marking the positions of the quadrature-path sampling instants $t_{nd}$ for $T_S = T_{\rm LO}/2$ and $T_D = T_S/2$. In Fig. 2(b) and (c), $T_S$ is increased by multiples of $T_{\rm LO}/2$, whereas $T_D$ is fixed at $T_S/2$. Note that $\sin(2\omega_{\rm LO}t_{nd}) = 0$ in Fig. 2(b) and (c). In Fig. 2(b) (i.e., for $T_S = T_{\rm LO}$), $\cos(2\omega_{\rm LO}t_{nd}) = 1$, and hence, $v_Q(t_{nd})$ in (8) reduces to 0, which is incorrect. However, in Fig. 2(c) (i.e., for $T_S = 3T_{\rm LO}/2$), $\cos(2\omega_{\rm LO}t_{nd}) = -1$, and hence, $v_Q(t_{nd})$ in (8) reduces to $x_{2Q}(t_{nd})$, which is the correct result. Therefore, when $T_D = T_S/2$, $v_Q(t_{nd})$ is nonzero, and time invariance is correctly maintained only when the sampling period $T_S$ is an odd multiple of $T_{\rm LO}/2$. This result can be generalized by introducing an additional design factor $k_D$ into the sampling constraint in (9) as follows:

$$T_S = k_D k_S \frac{T_{\rm LO}}{2}, \quad k_D = 1, 3, 5, \ldots; \quad k_S = 1, 2, 3, \ldots. \tag{11}$$

Using (11), the constraint on the quadrature-path sampling delay in (10) can be rewritten as

$$T_D = k_D \frac{T_{\rm LO}}{4}, \quad k_D = 1, 3, 5, \ldots. \tag{12}$$

Accordingly, the sampling period $T_S$ of an image-reject frequency-translating $\Delta\Sigma$ modulator (Fig. 1) must be selected using (11), and the quadrature-path sampling instants must be delayed by $T_D$ according to (12).

It is important to point out that the sampling constraints in (11) and (12) have been derived independent of the noise transfer function (NTF) of the inner-loop $\Delta\Sigma$ modulators and, therefore, can be applied to design image-reject frequency-translating $\Delta\Sigma$ modulators with continous-time (CT) or discrete-time (DT) lowpass or complex-bandpass inner-loop $\Delta\Sigma$ modulators. However, note that a complex-bandpass inner-loop $\Delta\Sigma$ modulator cannot be implemented with a DT loop filter, since the cross-coupled feedback paths of the complex integrators cannot be realized when the sampling instants of the in-phase and quadrature paths have different delays.

### C. DT Versus CT Inner-Loop $\Delta\Sigma$ Modulators

In Fig. 1, the outputs of the downconversion mixers contain both a low-frequency term (close to dc) and a high-frequency term (close to $2\omega_{\rm LO}$). Using DT inner-loop $\Delta\Sigma$ modulators [3], the in-phase and quadrature paths are sampled immediately following downconversion mixing, and the high-frequency term is subsampled to baseband. The quadrature-path sampling instants must therefore be delayed by $T_D$ relative to the in-phase path sampling instants [as per the constraint in (12)], to avoid cancellation of the low-frequency term by the subsampled high-frequency term.

In a frequency-translating $\Delta\Sigma$ modulator with CT inner-loop $\Delta\Sigma$ modulators [4], the high-frequency term is filtered by the signal transfer function of the CT inner-loop $\Delta\Sigma$ modulators and is attenuated prior to sampling. This implicit filtering makes it possible to realize an image-reject frequency-translating $\Delta\Sigma$ modulator with $T_D = 0$ (i.e., with the in-phase and quadrature paths sampled at the same time instants), where the sampling period $T_S$ is constrained by (9), rather than (11).

### D. General LO Signals

The sampling constraints in (11) and (12) have been derived assuming that the LO signals have the same phase as the sampling clock (i.e., $\theta_U = 0$ and $\theta_D = 0$ in Fig. 1). To verify that (11) and (12) are valid beyond this particular case, these constraints are applied to the outputs of the downconversion mixers, assuming that the LO signals have general phases $\theta_U$ and $\theta_D$ (Fig. 1). At sampling instants, this results in

$$v_I(t_n) = \cos(\theta_D)[\cos(\theta_U)x_{2I}(t_n) + \sin(\theta_U)x_{2Q}(t_n)] \tag{13}$$

$$v_Q(t_{nd}) = \cos(\theta_D)[\cos(\theta_U)x_{2Q}(t_{nd}) - \sin(\theta_U)x_{2I}(t_{nd})]\,. \tag{14}$$

As per (13) and (14), the sampled outputs of the downconversion mixers remain time invariant but now depend on phases $\theta_U$ and $\theta_D$. The phase $\theta_U$ of the LO signal that is applied to the upconversion mixers alters the response through the outer-loop path [6], whereas the phase $\theta_D$ that is applied to the downconversion mixer simply acts as a scaling factor.

A nonsinusoidal LO signal (e.g., the square wave generated by a switching mixer) introduces harmonics of the baseband spectrum at multiples of the LO frequency. When a nonsinusoidal LO signal is applied to the downconversion mixers, its harmonics are either subsampled (for DT inner-loop ΔΣ modulators) or attenuated (for CT inner-loop ΔΣ modulators) and, hence, have the same effect as a scaling factor. When a nonsinusoidal LO signal is applied to the upconversion mixers, its harmonics change the effective response through the outer-loop path. However, this change can be accounted for in the loop-filter design in the same way that an arbitrary DAC pulse shape is incorporated into the design of a classical CT ΔΣ modulator. Accordingly, the observations that were previously made for sinusoidal LO signals with arbitrary phase terms can be extended to general LO signals.

Observe that errors in the LO signals affect the NTF of a frequency-translating ΔΣ modulator in the same way that coefficient errors affect the NTF of a classical ΔΣ modulator. The impact of such errors, on the performance and stability of a frequency-translating ΔΣ modulator, becomes more significant as its out-of-band NTF gain is increased.

## III. Noise-Shaping Constraints

For stable operation, a ΔΣ modulator must be designed such that the signal content of its input can be adequately replicated by the signal content of its feedback path. This means that the low-frequency signal at the output of a frequency-translating ΔΣ modulator (Fig. 1) must be upconverted into the same band as the high-frequency signal at its input. This upconversion, as well as subsequent in-phase and quadrature path recombination at the input of the frequency-translating ΔΣ modulator, imposes basic constraints on the NTF of its inner-loop ΔΣ modulators, as described below.

### A. Lowpass Inner-Loop ΔΣ Modulators

Fig. 3 plots the magnitude response at four points along the feedback path of an image-reject frequency-translating ΔΣ modulator (Fig. 1) that has been designed with lowpass inner-loop ΔΣ modulators (assuming $f_S = f_{\mathrm{LO}}$): 1) at the sampled output $(y(n) = y_I(n) + jy_Q(n))$; 2) after the feedback DACs $(y(t) = y_I(t) + jy_Q(t))$; 3) after the upconversion mixers $(y_1(t) = y_{1I}(t) + jy_{1Q}(t))$; and 4) after in-phase/quadrature path recombination $(x_1(t))$. Note that Fig. 3(b) assumes a nonreturn-to-zero DAC, which has a magnitude response of the form $\sin(f)/f$ with notches at multiples of $f_S$ [6].

Observe that, in Fig. 3(d), the input-signal band contains only the desired signal and shaped quantization noise. Accordingly, there are no noise-shaping constraints for an image-reject frequency-translating ΔΣ modulator that uses lowpass inner-loop ΔΣ modulators.

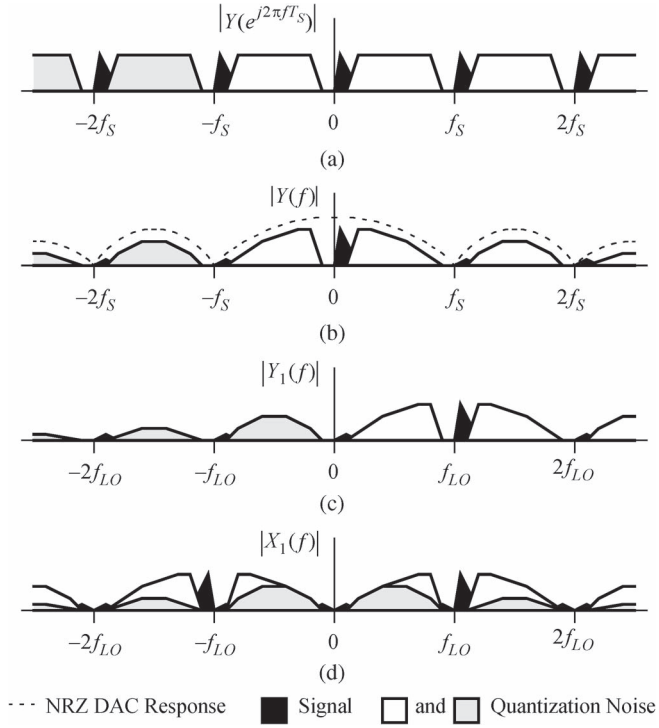


Fig. 3. Magnitude response along the feedback path of an image-reject frequency-translating ΔΣ modulator with lowpass inner-loop ΔΣ modulators: (a) at the sampled output $y(n)$; (b) after the DACs $y(t)$; (c) after upconversion mixing $y_1(t)$; and (d) after in-phase/quadrature path recombination $x_1(t)$.

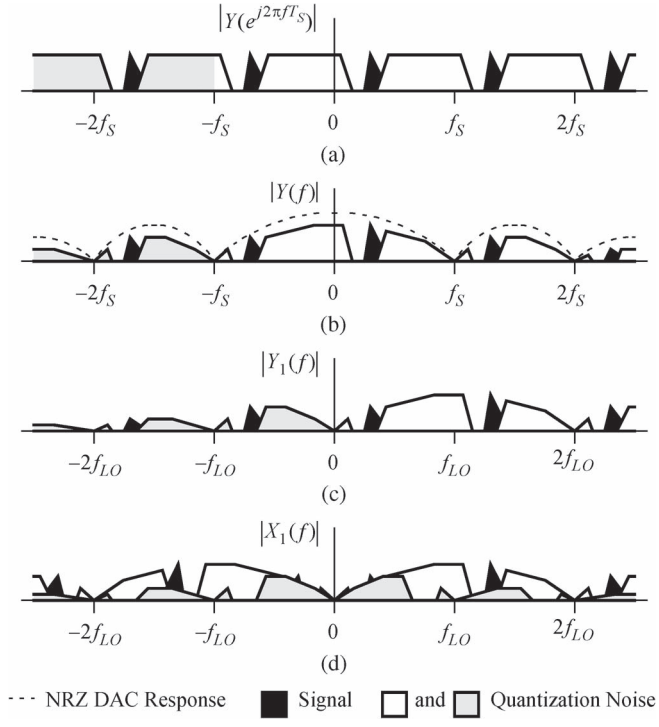


Fig. 4. Magnitude response along the feedback path of an image-reject frequency-translating ΔΣ modulator with a complex-bandpass inner-loop ΔΣ modulator: (a) at the sampled output $y(n)$; (b) after the DACs $y(t)$; (c) after mixing $y_1(t)$; and (d) after in-phase/quadrature path recombination $x_1(t)$.

### B. Complex-Bandpass Inner-Loop ΔΣ Modulators

Fig. 4 plots the magnitude response at the aforementioned points along the feedback path of a frequency-translating ΔΣ modulator (Fig. 1) that has been designed with a complex-bandpass inner-loop ΔΣ modulator (assuming $f_S = f_{\mathrm{LO}}$). Since the response of the complex loop filter is not

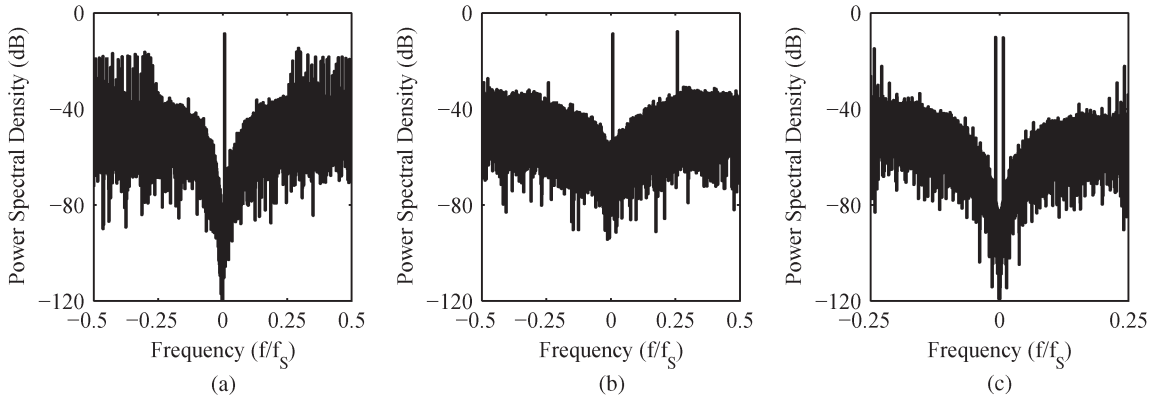


Fig. 5. Output spectrum of the image-reject frequency-translating $\Delta\Sigma$ modulator, which is simulated for (a) $T_S = 3T_{\rm LO}/2$, $T_D = T_{\rm LO}/4$ (i.e., $k_D = 1$ and $k_S = 3$), which satisfies the derived sampling constraints in (11) and (12); (b) $T_D = T_{\rm LO}/4$, but $T_S = 3.25T_{\rm LO}/2$, which violates the constraint in (11); and (c) $T_S = 3T_{\rm LO}/2$, but $T_D = 0$, which violates the constraint in (12).

symmetric about dc, quantization noise from the image band [close to $-5f_{\rm LO}/4$ in Fig. 4(c)] is translated into the input-signal band during in-phase and quadrature path recombination [Fig. 4(d)].

Performance loss can be minimized by filtering the quantization noise [in Fig. 4(b)] at an offset of approximately $-2f_{\rm LO}$ from the input-signal band prior to upconversion mixing. This can be achieved by increasing $k_S$ and reducing the center frequency at the $\Delta\Sigma$ modulator output to improve the filtering of the image band by the $\sin(f)/f$ response of the DACs.

## IV. Behavioral Simulation Results

An image-reject frequency-translating $\Delta\Sigma$ modulator (Fig. 1) was designed with first-order single-bit DT lowpass inner-loop $\Delta\Sigma$ modulators and simulated in SIMULINK. Circuit noise and nonlinearity were not considered in the behavioral simulation models. However, the effect of these nonidealities could be evaluated using standard techniques [10].

Fig. 5(a) plots the output spectrum of this $\Delta\Sigma$ modulator, with its sampling period set to $T_S = 3T_{\rm LO}/2$ (i.e., $k_D = 1$ and $k_S = 3$) to satisfy the constraint in (11), and with its quadrature-path sampling delay set to $T_D = T_{\rm LO}/4$ (i.e., $k_D = 1$) to satisfy the constraint in (12). The simulation results in Fig. 5(a) follow the expected noise-shaping performance of a fourth-order bandpass $\Delta\Sigma$ modulator [10], after accounting for the translated response of the outer-loop bandpass filter.

Fig. 5(b) plots the output spectrum of this $\Delta\Sigma$ modulator, with its sampling period changed to $T_S = 3.25T_{\rm LO}/2$, whereas $T_D = T_{\rm LO}/4$, as shown in Fig. 5(a). This choice of $T_S$ violates the constraint in (11) and causes certain terms of the loop response to oscillate at $f_S/4$, thus mixing quantization noise into the input-signal band.

Fig. 5(c) plots the output spectrum of this $\Delta\Sigma$ modulator, with its quadrature-path sampling delay changed to $T_D = 0$, whereas $T_S = 3T_{\rm LO}/2$, as shown in Fig. 5(a). This choice of $T_D$ violates the constraint in (12) and effectively reduces the output to a real spectrum.

## V. Conclusion

For the image-reject (quadrature) frequency-translating $\Delta\Sigma$ modulator, it has been demonstrated that: 1) the sampling period $T_S$ must be a multiple of $T_{\rm LO}/2$ to maintain time invariance, where $T_{\rm LO}$ is the period of the LO signal; 2) a sampling delay $T_D$ is required between the in-phase and quadrature paths that can be reduced to 0 for CT inner-loop $\Delta\Sigma$ modulators; and 3) the inner-loop $\Delta\Sigma$ modulators can utilize lowpass or complex-bandpass loop filters. However, the complex-bandpass case can only be implemented in CT and requires additional filtering.

## References

[1] R. Schreier, N. Abaskharoun, H. Shibata, D. Paterson, S. Rose, I. Mehr, and Q. Luu, "A 375-mW quadrature bandpass $\Delta\Sigma$ ADC with 8.5-MHz BW and 90-dB DR at 44 MHz," *IEEE J. Solid-State Circuits*, vol. 41, no. 12, pp. 2632–2640, Dec. 2006.

[2] V. S. L. Cheung and H. C. Luong, "A 3.3-V 240-MS/s CMOS bandpass $\Sigma\Delta$ modulator using a fast-settling double-sampling SC filter," in *Proc. Symp. VLSI Circuits Dig. Tech. Papers*, Jun. 2004, pp. 84–87.

[3] H. Tao and J. M. Khoury, "400-MS/s frequency translating bandpass sigma–delta modulator," *IEEE J. Solid-State Circuits*, vol. 34, no. 12, pp. 1741–1752, Dec. 1999.

[4] A. Pulincherry, M. Hufford, E. Naviasky, and U. K. Moon, "A time-delay jitter-insensitive continuous-time bandpass $\Delta\Sigma$ modulator architecture," *IEEE Trans. Circuits Syst. II, Exp. Briefs*, vol. 52, no. 10, pp. 680–684, Oct. 2005.

[5] A. Namdar and B. H. Leung, "A 400-MHz, 12-bit, 18-mW, IF digitizer with mixer inside a sigma–delta modulator loop," *IEEE J. Solid-State Circuits*, vol. 34, no. 12, pp. 1765–1776, Dec. 1999.

[6] A. I. Hussein and W. B. Kuhn, "Bandpass $\Sigma\Delta$ modulator employing undersampling of RF signals for wireless communication," *IEEE Trans. Circuits Syst. II, Analog Digit. Signal Process.*, vol. 47, no. 7, pp. 614–620, Jul. 2000.

[7] Y. Chen and K. T. Tiew, "A sixth-order subsampling continuous-time bandpass delta–sigma modulator," in *Proc. IEEE Int. Symp. Circuits Syst.*, May 2005, pp. 5589–5592.

[8] A. Kammoun, N. Beilleau, and H. Aboushady, "Undersampled $LC$ bandpass $\Delta\Sigma$ modulators with feedback FIRDACs," in *Proc. IEEE Int. Symp. Circuits Syst.*, May 2006, pp. 4427–4430.

[9] S. Reekmans, L. Hernandez, and E. Prefasi, "A subsampling quadrature $\Sigma\Delta$ modulator based on distributed resonators for use in radio receiver," *IEEE Trans. Circuits Syst. II, Exp. Briefs*, vol. 54, no. 9, pp. 820–824, Sep. 2007.

[10] R. Schreier and G. C. Temes, *Understanding Delta–Sigma Data Converters*. Piscataway, NJ: IEEE Press, 2005.